# Shape Factors for Irregularly-Shaped Matrix Blocks

Katha Wuthicharn, Robert W. Zimmerman, Imperial College London

**Abstract**

This paper presents shape factors (α) representing flow in fractured reservoir, including the shape factors for irregularly-shaped matrix blocks in both 2-Dimensional and 3-Dimensional flow. The shape factors are derived based on numerical simulation of fine-grid single porosity models. These numerical-estimated factors are verified with the known analytical values for available standard shapes i.e. square, circle and isosceles right triangle. As a result, an acceptable estimation is obtained with a maximum difference of 1%. Having achieved a verification for the standard shapes, the work is extended to irregular shape and 3D geometry. In addition, the paper introduces a new scaling law to estimate a universal constant value for dimensionless shape factor which can apply to any shape. The scaling law is derived from a combination of Darcy's law and Warren & Root's matrix-fracture flow model. The dimensionless shape factor, $\alpha \cdot \Delta l \frac{V}{S}$ gives the most confident value of $\alpha \cdot \Delta l \frac{V}{S} = 5.0$ with an error of less than 10%. The variable $\frac{V}{S}$ denotes volume-to-surface ratio of the matrix blocks while $\Delta l$ represents a characteristic length that similar to the mean radius of the pressure field; it is defined as $\Delta l \equiv \sqrt[2]{A}$ for 2D shape and $\Delta l \equiv \sqrt[3]{V}$ for 3D shape.

## Introduction

Naturally fractured reservoirs can be simplified as the reservoirs containing less-permeable matrix blocks surrounded by a network of interconnected high permeability fractures. Therefore, the system has high permeability contrast and these two porous media are interconnected and in communication. The most common approach to model naturally fractured reservoir is a dual (double) porosity model which firstly introduced by Barenblatt et al. (1960) and Warren and Root (1963). The mode is illustrated in figure 1 and 2. The dual porosity model treats matrix and fracture network as two continuous media where the transfer flux ($q_{mf}$) flowing between matrix and fracture is governed by a simple transfer function which was firstly proposed by Barenblatt (1960) as shown in the following equation:

$$\frac{Q(t)}{V} = q_{mf}(t) = \alpha \frac{k_m}{\mu} \left( \bar{P}_m - P_f \right) \qquad (1)$$

$q_{mf}$ represents volumetric flow rate of fluid flowing from the matrix blocks into the fractures per unit volume and has dimensions of volume flow rate per unit reservoir volume ($m^3/s \, / \, m^3$) or ($1/s$). This transfer flux should be inversely proportional to fluid viscosity but proportional to matrix permeability, pressure differential and shape factor ($\alpha$) of the system. This flow model is used in single phase flow in pseudo-steady-state where pressure gradient in matrix blocks is negligible and $\bar{P}_m$ represents matrix blocks average pressure. According to this equation, the drainage rate from the matrix to the fracture is controlled by the shape factor of matrix blocks and has the dimension of reciprocal area ($1/L^2$).

Warren and Root (1963) proposed the following expression for shape factor:

$$\alpha = \frac{4 N (N+2)}{L^2} \qquad (2)$$

N represents number of parallel sets of fractures i.e. slab column and cubes (N=1,2 or 3 respectively) and L denotes an average fracture spacing as illustrated in figure 1. For equal fracture spacing, the shape factor value of 1,2 and 3 sets are equal to $12/L^2$, $32/L^2$ and $60/L^2$ respectively. It is also suggested that L can be estimated from surface-volume ratio.

In the following decade, Kazemi et al. (1976) introduced a new shape factor formula developed by finite-different method, for three-dimensional case the formula is:

$$\alpha = 4 \left( \frac{1}{L_x^2} + \frac{1}{L_y^2} + \frac{1}{L_z^2} \right) \qquad (3)$$

If the assumption of equal fracture spacing is applied ($L_x = L_y = L_z$), the shape factor for value for one, two and three dimensional cases are equal to $4/L^2$, $8/L^2$ and $12/L^2$ respectively. The factor for three dimensional case is five-times less compare to Warren and Root's formula. The Kazemi's formula is widely used in dual porosity simulators. It should be noted that this formula is derived under the assumption of no pressure gradient within the matrix block. In addition, Ueda et al. (1989) explained that the equation 3 is equivalent to having linear pressure gradient between the center of a matrix block and the fracture.

A study on 3D shape factor of fine-grid single porosity and single-block dual porosity models by Thomas et al. (1989) concluded that the shape factor accounted for matrix pressure gradient for 3D case obtained from a good match between single and dual porosity model is $25/L^2$ of which the value is between Warren and Root's and Kazemi's model.

Coats (1989) proposed the shape factor exactly as large as twice of Kazemi's in his implicit compositional simulation work. In addition, he also derived an analytical solution of shape factor for constant rate boundary condition, the values for one, two and three sets of fractures are $12/L^2$, $28.45/L^2$, and $49.58/L^2$ respectively.

Udea et al. (1989) suggested the multiplication factors to the Kazemi et al. for one and two fracture sets. His work was conducted based on the comparison of single-porosity fine grid and dual porosity models. It concluded that Kazemi's shape factor need to be adjusted by factor of two and three for one and two fracture sets respectively.

Zimmerman et al. (1993) presented a correct analytical solution derived based on Fourier series analysis. In this work, a new shape factor for simple geometries are obtained by differentiating the most slowly decaying exponential term in the Fou-

rier series solution, eliminating t then comparing the result with the governing equation of Warren and Root. The shape factor for cubical is $\alpha=3\pi^2/L^2$, for column is $\alpha=2\pi^2/L^2$, for slab-like block is $\alpha=\pi^2/L^2$, for long cylindrical pipe radius $a$ is $\alpha=2.405^2/a^2$ or $23.14/D^2$ where 2.405 is the first positive root of Bessel function $J_0$ and finally the shape factor for spherical block is $\alpha=\pi^2/a^2$ where a is the mean radius of the block. In addition, Gottlieb (1988) also derived an analytical solution for isosceles right triangular prism using Laplace method, the shape factor is $\alpha=5\pi^2/L^2$ or $2.5\ \pi^2/A$ where A is the triangle's area.

Another work done by Zimmerman and Bodvarsson (1995) showed that the shape factor can be derived from the smallest eigenvalue of the Laplacian operator for region occupied by the matrix block. It is noted that only the shape factor for geometrically simple shape block can be directly derived from this theoretical approach.

For general case of three sets of orthogonal fracture and isotropic model, the shape factor is given by (Zimmerman and Bodvarsson,1995) the following equation (4). This equation was later confirmed by Lim and Aziz (1995) and was re-derived by Mathias and Zimmerman (2003) by Laplace transforms technique.

$$\alpha = \pi^2 \left( \frac{1}{L_x^2} + \frac{1}{L_y^2} + \frac{1}{L_z^2} \right) \tag{4}$$

Equation 4 can be reduced to $\alpha=\pi^2/L^2$ for one set of fracture or thin slab block having dimensions of $L_x=L$ where $L_y$, $L_z$ are very large ($L_y\ and\ L_z >> L$). For two sets of fracture or column having dimensions of $L_x= L_y =L$ and $L_z >> L$, $\alpha=2\pi^2/L^2$ and finally for three fracture sets or cubical shape where $L_x= L_y = L_z =L$, $\alpha=3\pi^2/L^2$.

For case of anisotropic reservoir, the shape factor is given as (Lim and Aziz, 1995) the following relation.

$$\alpha = \frac{\pi^2}{k} \left( \frac{k_x}{L_x^2} + \frac{k_y}{L_y^2} + \frac{k_z}{L_z^2} \right) \tag{5}$$

Mora and Wattenbarger (2009) investigated and reproduced the shape factor for all basic geometry by using both numerical and analytical methods. Their results confirmed the values introduced by Zimmerman et al. and Lim and Aziz. In addition, Mora also derived the shape factors for all basic geometry with constant rate boundary condition. The results are equivalent to Coats's figures (1989).

Although the correct solution for shape factor of simple geometry matrix block can be analytically obtained (Zimmerman et al. 1993), little research has been done for the case of shape factor for realistically-shaped matrix block.

In this work, a study on numerical-estimated shape factor is conducted for irregularly-shaped three dimensional blocks by fine-grid single porosity simulation. In order to achieve this ultimate goal, the numerical-derived shape factors for simple shapes such as column (two fracture sets), long-parallel pipe and isosceles right triangle prism are verified with the known analytical values and from this point, the standard procedure on estimating shape factor is developed.

In addition, this work investigates and develops a method to assign a shape factor for a matrix block based on its geometry and some characteristic length. In other words, this is a generic shape factor for the case where no analytical results are available and this generic value will be adopted without the need of fine-grid simulation.
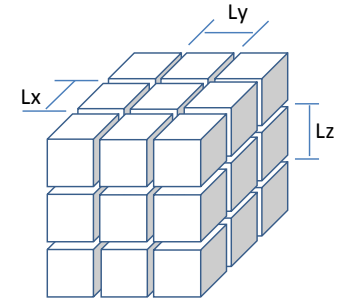


**Figure 1 A simplified matrix-fracture model for three normal fracture sets. (3D cubic shape)**

## A matrix-fracture pressure diffusion flow model and numerical simulation model
### Matrix-fracture flow model and pressure diffusion model

Fluid flow within a matrix block is governed by a simple mass balance within the matrix block where the rate of accumulation can be related to the matrix-fracture transfer rate. In our case, a pseudo-steady-state assumption is applied then the flow rate can be equated to the change in average matrix block pressure, then the following differential equation is obtained:

$$\emptyset_m\, c_m\, \frac{d\bar{P}_m}{dt} = \frac{\alpha\, k_m}{\mu} \left( P_f - \bar{P}_m \right) \tag{6}$$

The right term appears in this pressure diffusion equation (6) has the same form as equation (1) where the term represents unit volume flow rate between matrix-fracture coupling flow.

According to equation (6), $\emptyset_m$ represents porosity of matrix block, $c_m$ is total matrix compressibility which equals to the summation of pore compressibility ($c_p$) and fluid compressibility ($c_f$), $c_m = c_p + c_f$, $\bar{P}_m$ represents average matrix block pressure, $P_f$ is fracture pressure that equally distributes and surrounds the matrix block because of fracture high permeability, $k_m$ is matrix block permeability, $\mu$ is fluid viscosity and $\alpha$ represents shape factor of the system. The model is simplified and shown in figure 2.
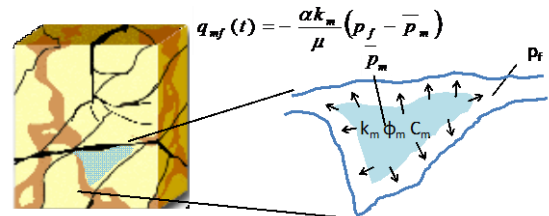


**Figure 2 A matrix-fracture pressure diffusion model.**

Equation 6 expresses the change in matrix pressure when there is a pressure differential between the fracture and the matrix, hence this pressure difference induces fluid flow between the two mediums. In reality, the close approximation for its appropriate boundary condition is a constant fracture pressure. This equation can be simply solved by assuming the constant fracture pressure ($P_f$ is constant) and gives the initial condition of matrix pressure with uniform pressure $P_m(t=0)=P_i$

$$\emptyset_m \, c_t \, \frac{d\bar{P}_m}{dt} = \frac{\alpha \, k_m}{\mu} \left( P_f - \bar{P}_m \right)$$

Rearrange the equation then;

$$\frac{1}{P_f - \bar{P}_m} d\bar{P}_m = \frac{\alpha \, k_m}{\emptyset_m \, \mu \, c_t} \, dt$$

For initial condition $P_m(t=0)=P_i$ and $P_f \equiv$ constant, integrate the equation from t=0 to t we get;

$$\int_{P_i}^{\bar{P}_m(t)} \frac{1}{P_f - \bar{P}_m} d\bar{P}_m = \frac{\alpha \, k_m}{\emptyset_m \, \mu \, c_t} \int_{t=0}^{t} dt$$

$$\mathrm{Ln}\left( \frac{P_f - \bar{P}_m(t)}{P_f - P_i} \right) = -\frac{\alpha \, k_m t}{\emptyset_m \, \mu \, c_t}$$

The solution to equation (6) subjects to the constant pressure boundary and its initial condition is

$$\frac{\bar{P}_m(t) - P_f}{P_i - P_f} = \exp\left( \left( -\frac{\alpha \, k_m}{\emptyset_m \, \mu \, c_t} \right) t \right) \qquad (7)$$

The term $\frac{\bar{P}_m(t) - P_f}{P_i - P_f}$ is known as normalised pressure (pD) and related to an exponent of a constant term on the right-hand side which represents a shape factor and other reservoir parameters as previously described. This equation (7) can be simply used to find the shape factor from numerical simulation by solving equation (6) with a reservoir simulator, Eclipse. The results are then computed to get average matrix pressure ($\bar{P}_m$) and normalised pressure (*pD*). Finally, the normalised pressure plotted against time (t) in semi-log plot will give the straight line which indicates pseudo-steady-state flow regime. The slope of this straight line (-m) represents a product of α and the term $\frac{k_m}{\emptyset_m \, \mu \, c_t}$, i.e.

$$\alpha = \frac{\emptyset_m \, \mu \, c_t}{k_m} \, m \qquad\qquad (8)$$

In other words, the pressure results from simulation can be simply visualised as a straight line by taking logarithmic on the equation (7), then we get;

$$Ln\left( \frac{\bar{P}_m(t) - P_f}{P_i - P_f} \right) = \left( -\frac{\alpha \, k_m}{\emptyset_m \, \mu \, c_t} \right) t \qquad\qquad (7\text{-}a)$$

### Numerical simulation model and methodology

In this study, the black oil simulator (Eclipse E100) was used to generate and simulate all models. The simulation work firstly started with developing fine-grid numerical simulation models for standard 2-dimelsional shape (2D), i.e. square, right isosceles triangle and circle then the work will be extended to irregular shape block and three dimensional (3D) blocks. For simple shape cases, the numerical-solved values are verified with the known analytical values in order to validate the models and make sure that they give correct results.

**Table 1 Simulation model parameters and initial condition**

| Input physical properties | Value | Field unit |
|---|---|---|
| Matrix porosity ($\varphi_m$) | 0.001 | |
| Fracture porosity ($\varphi_f$) | 0.90 | |
| Matrix initial pressure ($p_{mi}$) | 900 | psia |
| Fracture pressure ($p_f$) | 1000 | psia |
| Reservoir fluid | water | |
| Water viscosity ($\mu_w$) | 1 | c.p. |
| Water density ($\rho_w$) | 64 | lb/ft3 |
| Water compressibility ($c_w$) | 3.40E-06 | psi-1 |
| Rock compressibility ($c_p$ and $c_f$) | 3.40E-06 | psi-1 |
| Matrix permeability ($k_m$) | 1 | mD |
| **Simulation parameters** | **Value** | **Field unit** |
| Grid block size | 100x100x100 | feet |
| Depth of top reservoir | 10 | feet |
| Time step size | 0.01 | day |
| Number of time step | 1000 | step |

To simulate matrix-facture drainage flow, the grid architecture was constructed as a ring-like formation so that the matrix blocks are surrounded by fractures. Then the significant differential pressure between matrix and fracture are assigned to be 900 psia and 1000 psia respectively so that the reservoir fluid will flow from the fracture into the matrix. As discussed earlier that naturally fractured reservoir can be simplified as a reservoir containing less-permeable matrix surrounded by a network of interconnected high permeability fracture, for simulation purpose, the model's matrix permeability was made as small as 1 mD while it was 1000 mD for fracture region surrounding matrix, so that the fracture region would be in good pressure communication.

It is essential to keep fracture pressure as constant as possible to maintain the constant pressure boundary condition. To simulate this behaviour, the fracture pore volume needs to be as large as possible compare with the matrix; the fracture porosity was made to be 0.90 whereas it was 0.001 for matrix. Although porosity in nature reservoir cannot be as high as this value, this figure is used for simulating purpose and it does not distort the shape factor value in this study. A sufficiently large number of time steps were inputted so that the matrix blocks pressure can reach equilibrium pressure with the surrounding fracture. An acceptable final equilibrium pressure in this study should not be larger than 0.1% deviation from the initial fracture pressure. The other input physical properties and model initial condition are shown in table 1.
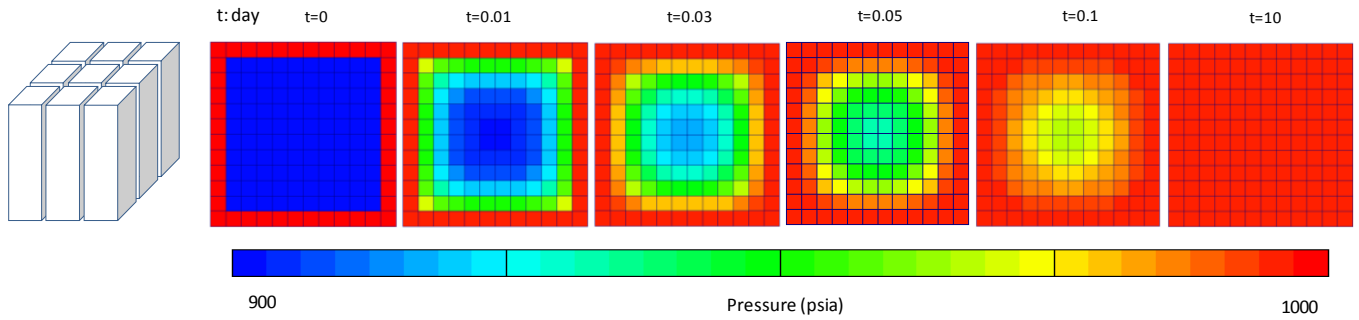
**Figure 3 A simplify model for two fracture sets (10x10 2Dsquare-shape) shows an initial condition and pressure diffusion until it reaches equilibrium.**

An example of fine-grid 2D square shape model with 100 matrix cells is used to illustrate and describe a standard methodology for model construction. The model consists of 10x10 matrix cells surrounded by ring of fracture cells and has the width of only one cell in the third dimension. The two systems have a significant pressure differential at initial condition. Figure 3 shows a standard 2D square-shape model, which is a simplified model for two fracture sets case (column geometry), at initial condition and at subsequent time steps. The initial pressure is assigned at 900 psia (blue) for the matrix and 1000 psia (red) for the fracture.

From this simulation, the pressure starts to diffuse until the two systems reach pressure equilibration at a final equilibrium pressure of 999.75 psia which is very close to the initial pressure, 1000 psia (0.03% deviation<<0.1%) as a result, the model satisfies constant pressure boundary condition. It can be seen that pressure diffuses very rapidly at early time and the diffusion shape at subsequent flow regime is symmetric as expected.

The average matrix pressure diffusion is plotted against time (blue line) in the figure 4, pressure diffuses faster during the early time compared to the late time regime where it gradually reaches the final pressure equilibration. The normalised pressure is computed and fitted with exponential function on semi-log plot as shown in equation (7) and the shape factor of the square shape can be obtained from this exponent by equation (8). Figure 5 shows the normalised pressure trend (red line) plotted against time on semi-log scale, the exponent denotes the product of α and the term $\frac{k_m}{\phi_m \mu c_t}$. The red curved line at early time regime ($t<<0.1$) represents a short transient period followed by a straight line trend which indicates pseudo-steady-state pressure diffusion regime.
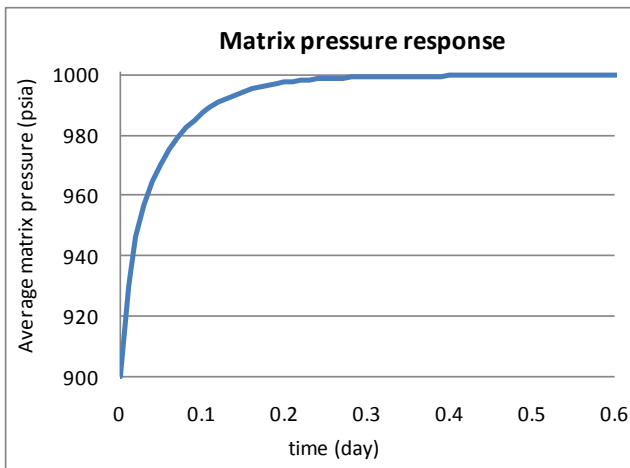


**Figure 4 An average matrix pressure trend for 10x10 square model. The initial matrix blocks pressure is 900 psia while it is 1000 psia in the fracture. The trend finally reaches a pressure equilibration at 999.8 psia which is sufficiently close to the fracture pressure (0.03% deviation) so a constant pressure boundary condition is maintained.**
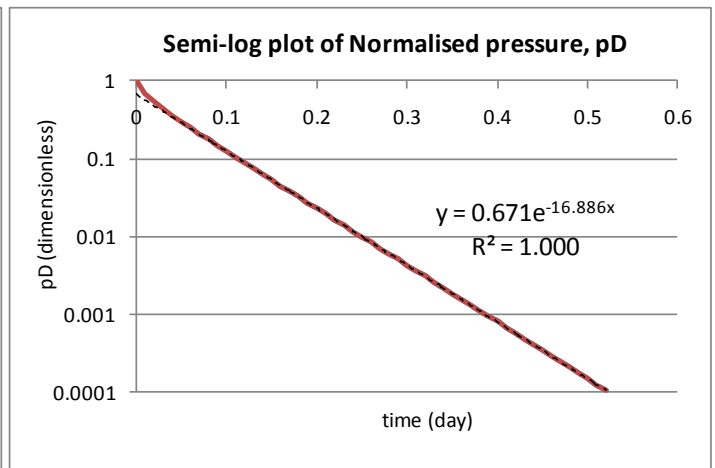
**Figure 5 Normalised pressure plotted on semi-log scale. The red curved line at early time regime (t<<0.1) represents a short transient period followed by an exponentially-fitted straight line which represents pseudo-steady-state pressure diffusion regime. The exponent term depends on shape factor of the matrix block as shown in eq.8.**

In this example, the shape factor (α) obtained from the exponent is 1.94e-4 $m^{-2}$ or $\alpha L^2$ is 18.10, where $L$ in this case is $L$=1000 ft (or $L\approx304.804$ m) and $L_x=L_y=L$ for the square shape, whilst the value is reasonably close to the analytical value of $2\pi^2$ or 19.74, with the deviation of 8.3%.

### Extrapolation technique to minimise grid resolution effect

Since the shape factor of square shape obtained from the previous example deviates from the theoretical value significantly so it is essential to have the finer grid model to get the closer estimation. There are three additional grid resolution models for the square shape i.e. 12x12, 20x20 and 28x28 cells. Having computed $\alpha L^2$ for each case, the extrapolation technique adapted from Yeo and Zimmerman (2000) is then used to extrapolate the number of cells to reach infinity so that this extrapolated shape factor, $\alpha_e L^2$ is finally converged to the theoretical value. The $\alpha L^2$ for each case are plotted against $1/N$, where $N^2$ represents number of matrix cells, $\alpha L^2$ value is then extrapolated down to $1/N=0$ where it represents infinite cells. The $\alpha_e L^2$ value obtained from the y-interception is 19.63 as shown in the figure 6 below. The deviation is as small as 0.56% from the theoretical value. From the fitted curve line shown in the graph, the downward trend line also implies that the extrapolation converges to a single value when $1/N$ reaches zero. Ideally, the curve reaches its maximum value at this point as the trend of $\alpha L^2$ increases while $1/N$ reduces according to the graph.
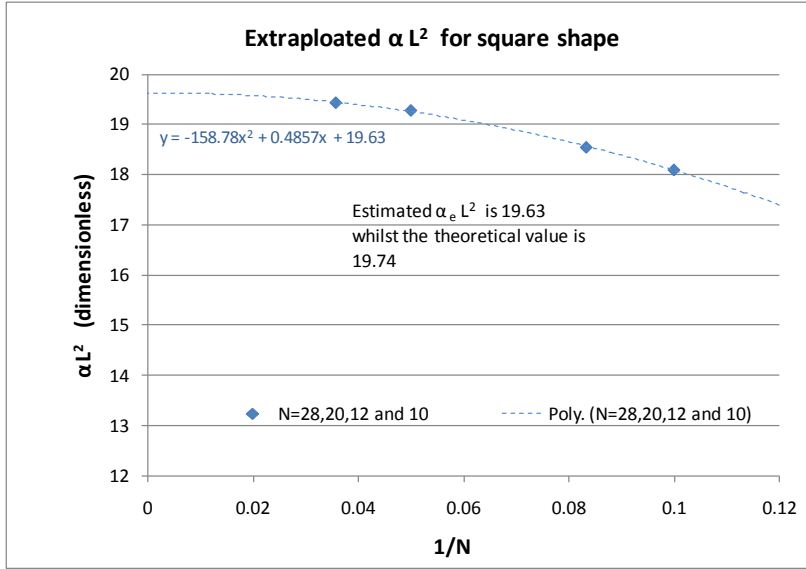


Figure 6 Extrapolation technique used to estimate shape factor more accurately by extending number of cells to infinity ($1/N \rightarrow 0$). In this example, an extraploation of the shape factor for 2D square shape give $\alpha L^2$ of 19.63 whereas the analytical solution is $2\pi^2$ or 19.74
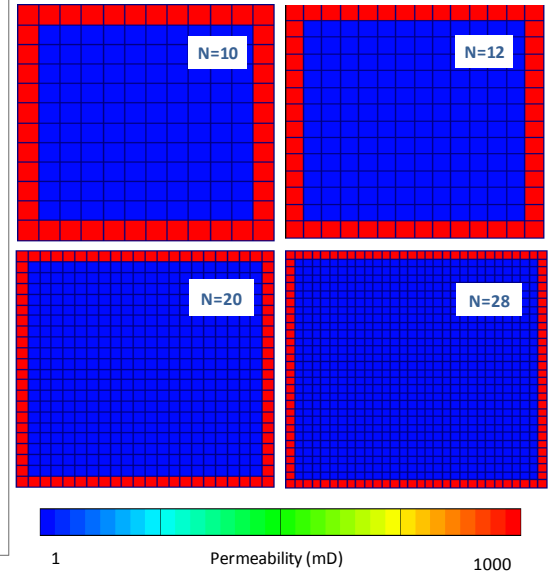


Figure 7 2D square simulation models of different grid resolution. The models give the slightly different shape factors due to grid resolution effect.

## Shape factor for 2-Dimensional geometry

### Shape factor for square shape (long-column geometry)

A numerical-estimated $\alpha L^2$ for the case of a square shape is 19.63 whereas the analytical value is $2\pi^2$ or 19.74. The numerical value obtained from fine-grid model and extrapolation technique gives an acceptable result with 0.56% difference. Table 2 summarises the numerical-estimated shape factor values of square geometry for different grid resolutions and the final equilibrium pressure based on these models.

Table 2 Equilibrium pressure and the numerical-estimated shape factor of 2D square shape for different grid resolution models, the more number of cells give more accurate value i.e. for N=28 the value approaches the analytical solution.

| Case | $\alpha$ (1/m$^2$) | $\alpha L^2$ | 1/N | Equilibrium pressure | % pressure deviation |
|---|---|---|---|---|---|
| square N=10 | 1.95E-04 | 18.10 | 0.100 | 999.748 | 0.03% |
| square N=12 | 1.39E-04 | 18.55 | 0.083 | 999.693 | 0.03% |
| square N=20 | 5.19E-05 | 19.28 | 0.050 | 999.474 | 0.05% |
| square N=28 | 2.67E-05 | 19.43 | 0.036 | 999.322 | 0.07% |

### Shape factor for circular shape (cylindrical parallel pipe or radial flow geometry)

The long-parallel pipe represents radial flow geometry can be simplified to a 2D circular shape as shown in figure 8. Three numerical simulation models of different grid resolutions with $N$=15, 21 and 31 were constructed in the same way of the square shape. Since the circular-shape hypotenuse is formed by number of fine-square grids, it requires larger amount of cells to form these circle models compare to the first example of square shape as shown in figure 7 and 9. The model has a diameter as its characteristic length, so for circular shape N denotes number of grid which forms a diameter. Table 3 shows the numerical-computed value of $\alpha L^2$ and the final equilibrium pressure for each model. Noted that $\alpha L^2$ converges to the analytical value when the model has finer grid. Because the models have larger number of matrix cells so it is necessary to reduce matrix porevolume to maintain constant pressure boundary in the fracture and hence the porosity value is reduced by factor of ten for

the circle-shape models. From this table, the final equilibrium pressure approaches 1000 psia with the deviation of only 0.002%, as a result, the boundary pressure is constantly maintained.
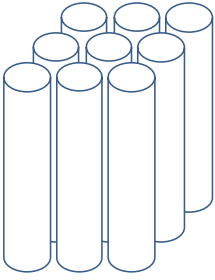


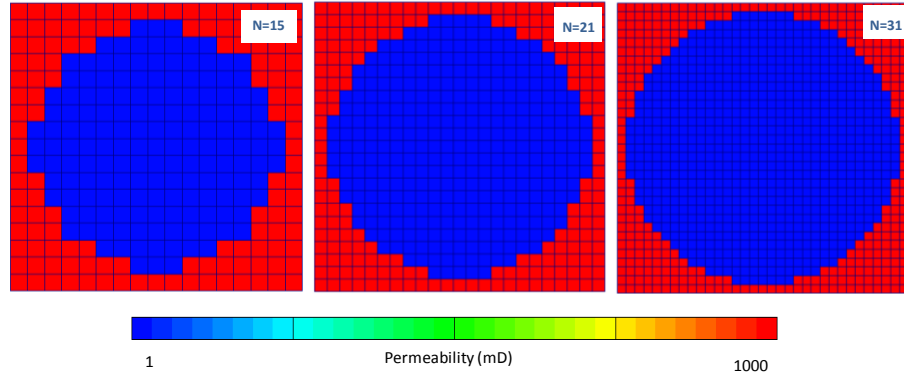**Figure 8 Long-parallel pipe model: the model is simplified to 2D circular shape**

**Figure 9 2D circle models for different grid resolution i.e. N=15, 21 and 31. The finer grid give the more accurate shape factor compare to the analytical value.**

**Table 3 Equilibrium pressure and the numerical-estimated shape factor of 2D circular models for different grid resolution.**

| Case | $\alpha$ (1/m$^2$) | $\alpha L^2$ | 1/N | Equilibrium pressure | % pressure deviation |
|---|---|---|---|---|---|
| circle N=15 | 1.18E-04 | 17.60 | 0.067 | 999.987 | 0.001% |
| circle N=21 | 5.73E-05 | 17.73 | 0.048 | 999.983 | 0.002% |
| circle N=31 | 2.57E-05 | 17.83 | 0.032 | 999.978 | 0.002% |

The extrapolation of $\alpha L^2$ for circular shape is plotted in figure 10. $\alpha L^2$ computed from different grid resolution models were extrapolated against *1/N*. The numerical-estimated shape factor ($\alpha L^2$) for the case of a square shape is 17.99 whereas the analytical value is 18.17. Noted that some authors report the analytical alpha of *23.14/D$^2$* or it is equivalent to *18.17/L$^2$* if the area is used as a scaling parameter instead of the diameter. The numerical value obtained from fine-grid model and extrapolation technique gives an acceptable result with 0.97% discrepancy. The circular shape factor is slightly less than that of the square. This is logical since the circle has shorter perimeter to the square of the same area. This idea will be expanded when it comes to scaling law section.
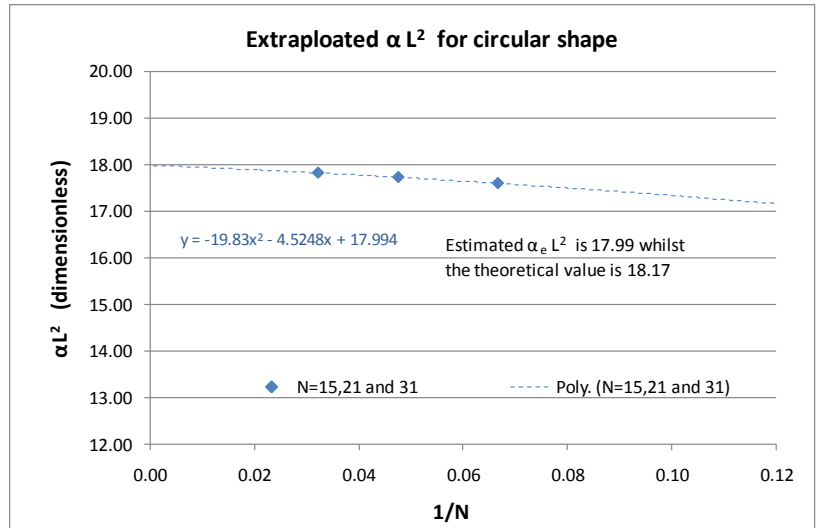


**Figure 10 Extrapolation of the shape factor for 2D circular shape, the estimated $\alpha L^2$ is 17.99 whilst the analytical solution is 18.17.**

### Shape factor for isosceles right triangle (one diagonal fracture addition to the square shape)

Right isosceles right triangle is a simplified model for a matrix-fracture system that contains three fracture sets of which an additional diagonal fracture superimposes on the square geometry. The same methodology was applied to obtain $\alpha L^2$ for this flow geometry. The shape factor of four different grid resolution models of *N*=6, 10, 14 and 20 were computed and extrapolated to get an extrapolated final $\alpha L^2$. Note that the triangular shape model is not a perfect triangle because it is formed by number of small square cells, in fact it is a staircase-shaped hypotenuse model as see in the figure11.

**Table 4 Equilibrium pressure and the numerical-estimated shape factor of isosceles right triangle models for different grid resolution.**

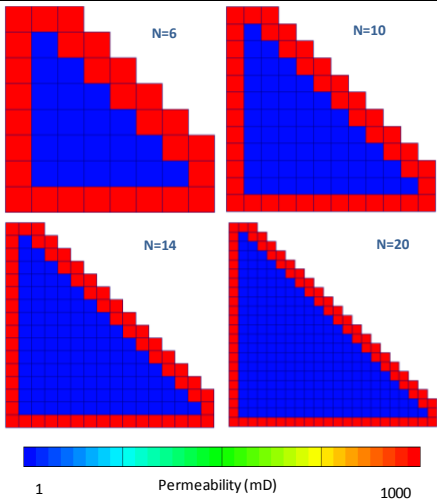| Case | $\alpha$ (1/m$^2$) | $\alpha L^2$ | 1/N | Equilibrium pressure | % pressure deviation |
|---|---|---|---|---|---|
| isosceles right triangle N=6 | 1.11E-03 | 21.73 | 0.167 | 999.924 | 0.008% |
| isosceles right triangle N=10 | 4.55E-04 | 23.23 | 0.100 | 999.874 | 0.013% |
| isosceles right triangle N=14 | 2.46E-04 | 23.95 | 0.071 | 999.824 | 0.018% |
| isosceles right triangle N=20 | 1.23E-04 | 24.07 | 0.050 | 999.738 | 0.026% |

**Figure 11 Isosceles right triangle models for different grid resolution i.e. N=6, 10, 14 and 20**
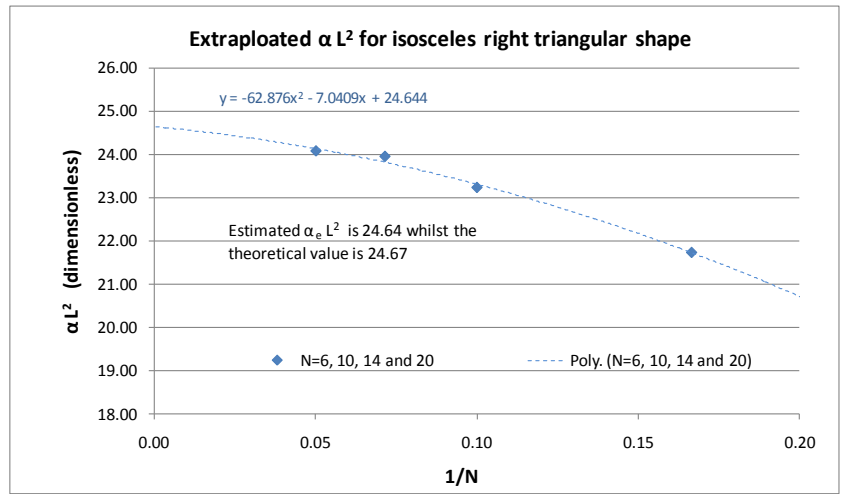


**Figure 12 Extrapolation of the shape factor for 2D Isosceles right triangle, the estimated $\alpha L^2$ is 24.64 whilst the analytical solution is 24.67.**

The results for each simulation model are tabulated in the table 4. The final equilibrium pressure approaches the initial fracture pressure followed constant pressure condition. The maximum pressure deviation is only 0.026% for *N*=20.

The extrapolation curve for the right triangular shape is shown in the figure 12. In the like manner as square and circle, the extrapolated value converges to a single value which is very close to the theoretical value. For this case, an extrapolated $\alpha L^2$ is 24.64 whereas the analytical value based on area scaling is *2.5π²* or 24.67. In other words, the deviation is as small as 0.12%.

From verification of the standard shapes i.e. square circle and isosceles right triangle, the numerical-derived shape factor values are accurately estimated compared to the analytical values. So the methodology can be applied and extended to 2D irregular shape and 3D modelling.

### Shape factor for 2D irregularly-shaped matrix blocks

Having obtained numerical-estimated shape factor for standard shapes, the work is extended to 2D irregular shape. The shape was designed as a combination of square and triangle; in other words, it is neither so close to the rectangle or triangle as shown in figure 13. Because the model shape is irregular where there is no analytical solution, it is unnecessary to construct several models and extrapolate as done in the previous shapes. In addition, it is not easy to get the high level of model similarity with different grid resolutions for irregular shape. As a result, to avoid the need of having more than one model for extrapolation, the model was designed so it contains as much cells as possible. Table 5 shows the detail of model parameters and its initial condition. In addition, the simulation results of final equilibrium pressure and the shape factor are tabulated in the table 6.

**Table 5 Model parameters and initial condition for 2D irregular shape**

| Input physical properties | Value | Field unit |
|---|---|---|
| Matrix porosity ($\varphi_m$) | 0.0001 | |
| Fracture porosity ($\varphi_f$) | 0.99 | |
| Matrix initial pressure ($p_{mi}$) | 900 | psia |
| Fracture pressure ($p_f$) | 1000 | psia |
| Fracture permeability ($k_f$) | 1000 | mD |
| Matrix permeability ($k_m$) | 1 | mD |
| **Simulation parameters** | **Value** | **Field unit** |
| Number of cells in the model | 510 | cell |
| Number of matrix cells | 199 | cell |
| Number of fracture cells | 311 | cell |
| Grid block size | 100x100x100 | feet |
| Depth of top reservoir | 10 | feet |
| Time step size | 0.0001 | day |
| Number of time step | 2000 | step |
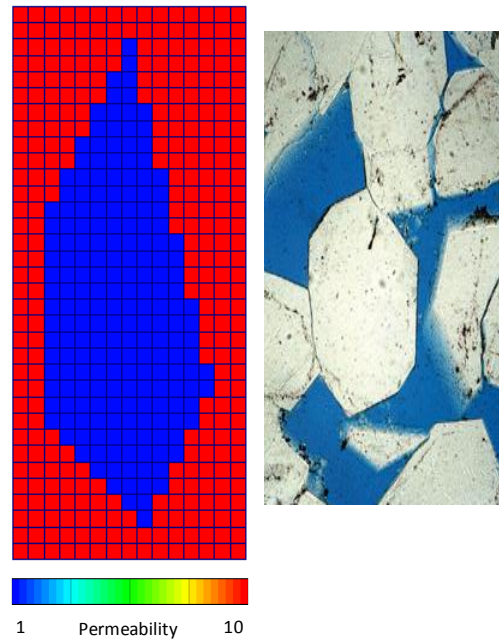


**Figure 13 Grid architecture for 2D irregular shape matrix blocks adapted from actual irregular blocks in thin section view**

**Table 6 Simulation results for 2D irregular shape**

| Parameter | Value |
|---|---|
| $\alpha$ (1/m²) | 1.43E-04 |
| $\alpha L^2$ | 26.42 |
| Equilibrium pressure (psia) | 999.994 |
| % pressure deviation | 0.001% |

According to the results, the dimensionless shape factor, $\alpha L^2$ is estimated to be 26.42 which is quite similar to that of the right triangle since the irregular shape can split into small triangles. The final equilibrium pressure satisfies the constant pressure boundary condition, the deviation is only 0.001%.

## Scaling laws for a generic shape factor: 2D geometry

As previously mentioned, the ultimate goal of this work is to estimate a generic shape factor value which can be applied to any matrix shape without the need of fine-grid numerical simulation. This value should be estimated based on some representative scaling technique and should gives the minimum deviation. For this work, a single universal value with a deviation of 10% is considered as an acceptable figure. In other words, this generic constant must be compared to the known analytical solution value and give an error of less than 10%.

The scaling technique starts with the matrix-fracture flow equation (1) where $\frac{Q(t)}{V}$ represents a unit-volume flow rate:

$$\frac{Q(t)}{V} = q_{mf}(t) = \alpha \, \frac{k_m}{\mu} \left( \bar{P}_m - P_f \right)$$

The total flux flowing from fracture to matrix is:

$$Q(t) = \alpha \, V \, \frac{k_m}{\mu} \left( P_f - \bar{P}_m \right) \qquad (1\text{-}a)$$

The volumetric flow rate for the typical fracture system for a single phase can be expressed by Darcy's law, therefore:

$$Q(t) = \frac{k_m}{\mu \, \Delta l} S \left( P_f - \bar{P}_m \right) \qquad (9)$$

Where $S$ denotes the *outer surface area* of the matrix and $\Delta l$ is a characteristic length that represents mean path line of the flow field between the point of average pressure in matrix (centroid of the pressure field within matrix) and the surrounding fracture where the pressure maintains constant. In other words we can imagine that $\Delta l$ is a characteristic length that similar to the mean radius of the flow field.

Assign (1-a) = (9) hence:

$$\alpha = \frac{(S/V)}{\Delta l} \qquad (10)$$

Equation (10) has dimension of reciprocal area ($1/m^2$), the term $S$ denotes the outer surface area of the matrix, $V$ is the matrix volume and $\Delta l$ is a characteristic length that represents a path line of the flow between the point of average pressure in matrix (centroid of the pressure field within matrix) and a point in the surrounding fracture where the pressure maintains constant. In other words we can imagine that $\Delta l$ is a characteristic length that is similar to the mean radius of the flow field. Equation (10) cannot directly apply because the characteristic length $\Delta l$ cannot be explicitly found from the shape geometry. Nevertheless, the expression gives an instructive view of how $\alpha$ depends on geometry of the matrix block. One of a simple example for 3D shape is a cubical shape which has an equal length of $L$. In this case, $S/V$ is $6L^2/L^3 = 6/L$ and $\Delta l$ can be simplified to $\sqrt[3]{V}$ or $L$ and hence the dimensionless alpha, $\alpha \, \Delta l \, \frac{V}{S} = \alpha \, \frac{L^2}{6}$. The term $\alpha L^2$ can be obtained from the numerical simulation as a result $\alpha \, \Delta l \, \frac{V}{S}$ is then computed explicitly. The first scaling law to get a dimensionless alpha is $\alpha \, \Delta l \, \frac{V}{S}$

For 3D shape: $\Delta l \equiv \sqrt[3]{V} \qquad (11)$

Hence $\alpha \cdot \Delta l \, \frac{V}{A}$ becomes $\alpha \cdot (V^{\frac{4}{3}}/A)$

For the case of 2D shape, the surface area ($S$) is the product of Perimeter ($\Pi$) and width ($w$) i.e. $S = \Pi \cdot w$ and similarly $V = A \cdot w$ and hence the term $S/V = \Pi/A$. The term $\Delta l$ can be simplified to $\sqrt[2]{A}$ and hence $\alpha \cdot \Delta l \, \frac{V}{S}$ becomes $\alpha \cdot (A^{1.5}/\Pi)$.

For 2D shape: $\Delta l \equiv \sqrt[2]{A} \qquad (12)$

Apart from this scaling technique, there are number of ways to create scaling factors to get the dimensionless alpha. The key idea is that the scaling parameters must have a dimension of length square ($L^2$) so that the multiplication term of scaling factor and alpha becomes dimensionless. In this work, there are four scaling factors being investigated i.e. area ($A$), perimeter square ($\Pi^2$), $(A/\Pi)^2$ and $\Delta l \, \frac{V}{S}$. The scaled alpha in dimensionless form for 2D shapes is tabulated in the table 7.

**Table 7 Scaling laws to estimate dimensionless shape factor of various geometries for 2D model**

| Matrix Shape | $\alpha A$ | $\alpha \Pi^2$ | $\alpha (A/\Pi)^2$ | $\alpha (A^{1.5}/\Pi)$ or $\alpha \cdot \Delta l \frac{V}{S}$ | Deviation from average | | | |
|---|---|---|---|---|---|---|---|---|
| | | | | | $\alpha A$ | $\alpha \Pi^2$ | $\alpha (A/\Pi)^2$ | $\alpha (A^{1.5}/\Pi)$ or $\alpha \cdot \Delta l \frac{V}{S}$ |
| Square | 19.63 | 314.1 | 1.23 | 4.91 | -11% | -37% | 9% | 0% |
| Isosceles right triangle | 24.64 | 574.5 | 1.06 | 5.10 | 11% | 14% | -6% | 4% |
| Circle | 17.99 | 226.1 | 1.43 | 5.07 | -19% | -55% | 27% | 3% |
| Irregular shape2D | 26.42 | 892.6 | 0.78 | 4.55 | 19% | 78% | -30% | -7% |
| average | 22.17 | 501.8 | 1.12 | 4.91 | | | | |
| standard deviation (S.D.) | 4.00 | 299.61 | 0.28 | 0.26 | | | | |
| S.D. and mean % diff. | *18%* | *60%* | *24%* | *5%* | | | | |

According to the table, if the area (*A*) is used as a scaling parameter, the dimensionless values vary between 17.99 (circle) and 26.42 (irregular shape) with a deviation of +-19% from the average value and the standard deviation of 18%. For the case of the perimeter square ($\Pi^2$), the standard deviation goes up to 60% while it is 24% for the case of $(A/\Pi)^2$. In other words, these two scaling factors are not as good as the area. Finally, if the scaling factor is $A^{1.5}/\Pi$ (or $\Delta l \frac{V}{S}$), the variation is minimum i.e. only 7% . Therefore, it can conclude that using $A^{1.5}/\Pi$ (or $\Delta l \frac{V}{S}$) as a scaling parameter gives the smallest error (7%) with only 5% of the standard deviation.

## Shape factor for 3-Dimensional geometry

Having achieved an estimation of a generic dimensionless shape factor for 2D shape, the work is extended to 3D geometry. The simplest 3D geometry is cubical shape so it was used as a testing model against the known analytical solution. The numerical simulation model for 3D cube was constructed by following the standard procedure done in the 2D shape. Apart from 3D cube, an additional model for a 3D equilateral square pyramid was constructed to find the shape factor. And finally, a 3D irregular shape model, as a key experiment, is modeled and tested against the scaling law to obtain a universal constant for dimensionless shape factor.

### Shape factor for 3D cubical shape (a reservoir having three normal fracture sets)

The model architecture for a 3D cube is based on the same idea that of 2D shape; the simulation model consists of matrix cells surrounded by fracture shell as shown in figure 14. The model properties and its initial condition are tabulated in table 8.

**Table 8 Input parameters for 3D cube simulation model**

| Input physical properties | Value | Field unit |
|---|---|---|
| Matrix porosity ($\varphi_m$) | 0.0001 | |
| Fracture porosity ($\varphi_f$) | 0.99 | |
| Matrix initial pressure ($p_{mi}$) | 900 | psia |
| Fracture pressure ($p_f$) | 1000 | psia |
| Matrix permeability ($k_m$) | 1 | mD |
| Fracture permeability ($k_f$) | 1000 | mD |
| Reservoir fluid | water | |
| Water viscosity ($\mu_w$) | 1 | c.p. |
| Modified water density ($\rho_w$) | 0.624 | lb/ft3 |
| Water compressibility ($c_w$) | 3.40E-06 | psi-1 |
| Rock compressibility ($c_p$ and $c_f$) | 3.40E-06 | psi-1 |
| **Simulation parameters** | **Value** | **Field unit** |
| Number of cells in the model | 12x12x12 | cell |
| Number of matrix cells | 10x10x10 | cell |
| Number of fracture cells | 728 | cell |
| Grid block size | 1x1x1 | feet |
| Depth of top reservoir | 10 | feet |
| Time step size | 0.0001 | day |
| Number of time step | 2000 | step |
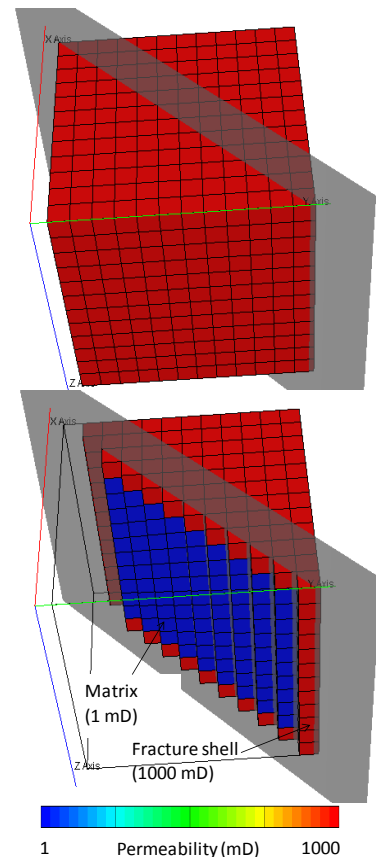


**Figure 14 3D cube model cross-sectional view shows matrix and fracture permeability.**

**Table 9 Simulation results for 3D cubic shape**

| Parameter | Value |
|---|---|
| $\alpha$ (1/m$^2$) | 3.14 |
| $\alpha L^2$ | 29.15 |
| $\alpha L^2$ (theoretical value) | 29.61 |
| Equilibrium pressure (psia) | 999.985 |
| % pressure deviation | 0.001% |

According to table 9, the simulation results show that the 3D cubical model satisfies a constant pressure boundary condition and the final equilibrium pressure deviates from initial pressure only 0.001%. The model gives a numerical-derived $\alpha L^2$ of 29.15 whereas the analytical solution is $3\pi^2$ or 29.61 that is the deviation of 1.5%. Note that $L$ denotes cubical root of volume or the length of each side for this particular 3D cube model. This model is equivalent to a fracture reservoir having three normal fracture sets as shown in figure 1.
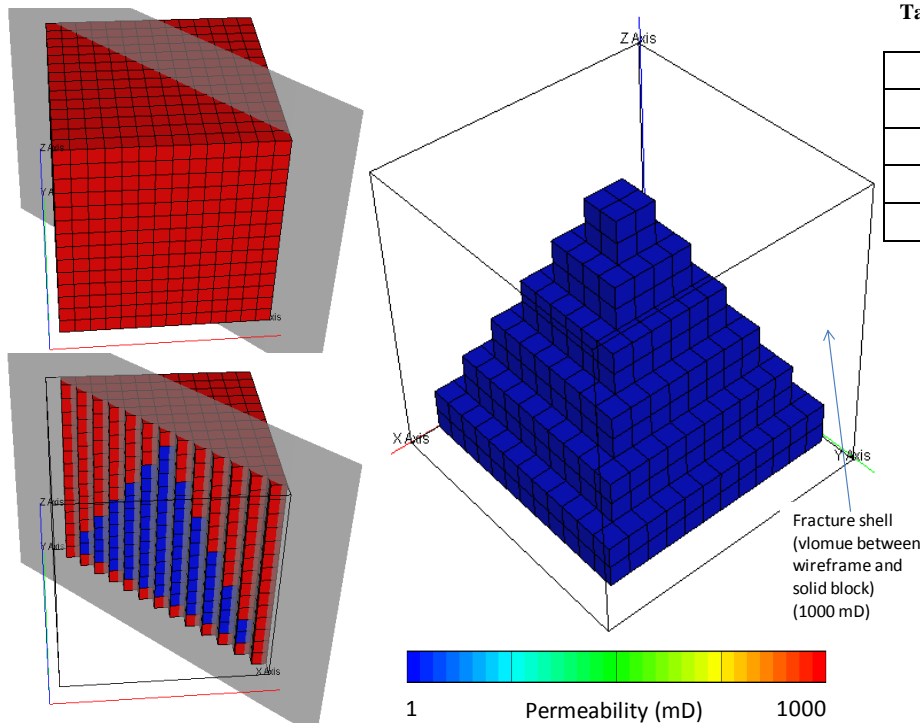
### Shape factor for 3D equilateral square pyramid

A model of 3D square pyramid with all four side-faces of equilateral triangles was constructed to find a shape factor for testing the scaling law. The model consists of small cells form a staircase-shaped hypotenuse pyramid as shown in the figure 15. The model basic properties are the same as that of 3D cube model as shown in table 10.

Table 11 shows the numerical-derived shape factor for 3D square pyramid. The model gives $\alpha L^2$ of 33.33 and the final equilibrium pressure is very close to 1000 psia so a constant pressure condition is maintained as expected.

**Table 10 Input parameters for 3D square pyramid model**

| Simulation parameters | Value | Field unit |
|---|---|---|
| Number of cells in the model | 14x14x14 | cell |
| Number of matrix cells | 728 | cell |
| Number of fracture cells | 2016 | cell |
| Grid block size | 1x1x1 | feet |
| Depth of top reservoir | 10 | feet |
| Time step size | 0.0001 | day |
| Number of time step | 2000 | step |



**Table 11 Simulation results for 3D square pyramid**

| Parameter | Value |
|---|---|
| $\alpha$ (1/m$^2$) | 4.43 |
| $\alpha L^2$ | 33.33 |
| Equilibrium pressure (psia) | 999.989 |
| % pressure deviation | 0.001% |

Fracture shell
(vlomue between
wireframe and
solid block)
(1000 mD)

1          Permeability (mD)          1000

**Figure 15 3D square pyramid model cross-sectional view shows matrix and fracture permeability.**

### Shape factor for 3D irregularly-shaped matrix block

As the 3D cube model is formed by six orthogonal planes, similarly, a 3D irregularly-shaped model is formed by six oblique planes so the shape is like a tapered block as shown in figure 16 and 17. Figure 16 aims to illustrate the 3D irregular shape in different orthographic projection views so that the model's profile can be captured and the shape can be perceived. In addition, figure 17 explicitly illustrates the irregular shape by giving its x, y and z coordinates.
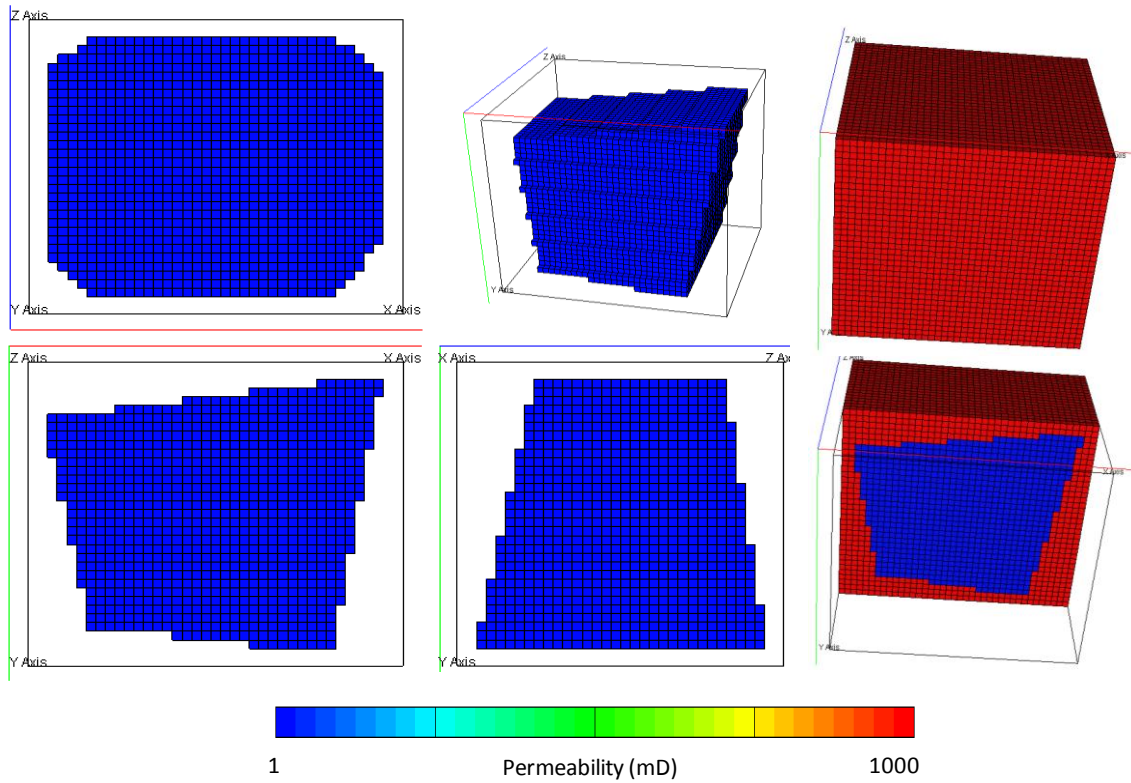
**Figure 16 Orthographic projections for 3D irregular shape showing the model's profile of the front, the top and the right views. The isometric and cross-sectional views are also included here.**
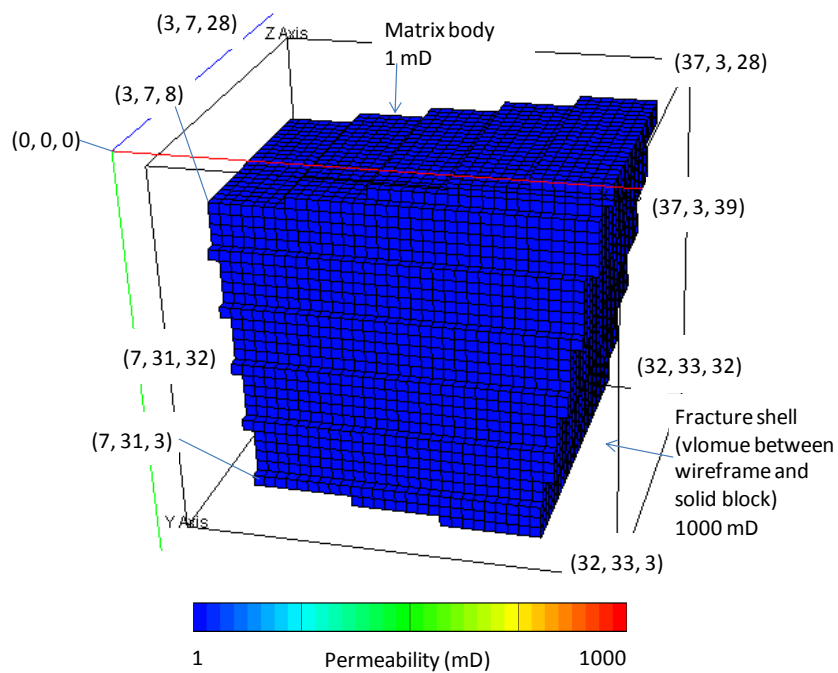


**Figure 17 Coordinates of 3D irregular shape model. The coordinate uses the Cartesian convention of x-axis (red), y-axis (green) and z-axis (blue).**

**Table 12 Input parameters for 3D irregular shape model**

| Simulation parameters | Value | Field unit |
|---|---|---|
| Number of cells in the model | 39x35x34 | cell |
| Number of matrix cells | 21075 | cell |
| Number of fracture cells | 46410 | cell |
| Grid block size | 1x1x1 | feet |
| Depth of top reservoir | 10 | feet |
| Time step size | 5.00E-09 | day |
| Number of time step | 2000 | step |
| Matrix volume | 21075 | ft3 |
| Surface area | 4595 | ft2 |

As the model is considered as a numerous models, the grid size is very small and the model contains large number of cells. Therefore, the time step is reduced to 0.0004 second (5e-9 day) in order to capture the early-time pressure response and to obtain the shape factor accurately. The time step and other simulation model parameters for 3D irregular shape are tabulated in table12. Note that model's volume and surface area are explicitly computed for uses in scaling law investigation.

According to the simulation results, the model's pressure response follows the constant pressure boundary condition and both early time and late time pressure data are valid as shown in figure 18. The recorded pressure trend is smooth and it follows exponential fit as see in figure 19.
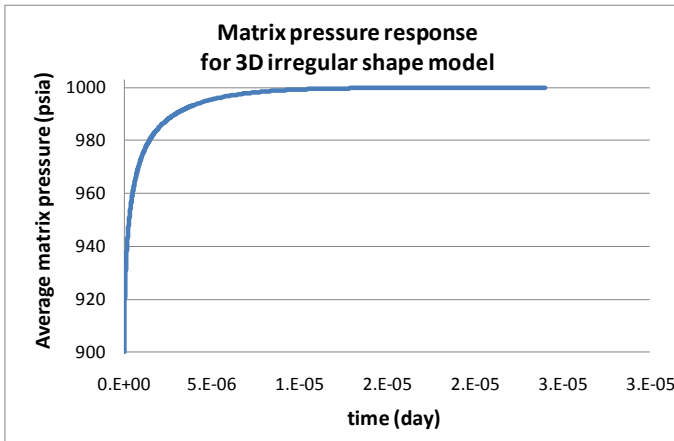


**Figure 18 Matrix-averaged pressure of 3D irregular shape model. The trend reaches pressure equilibration at 999.99 psia so the constant pressure boundary condition is maintained.**
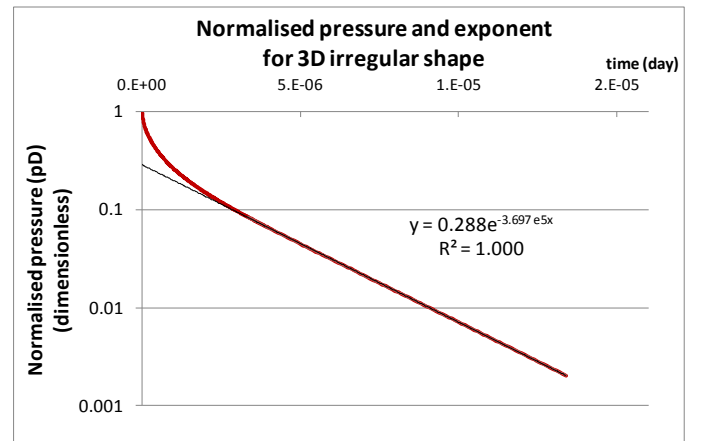


**Figure 19 A straight line trend of normalised pressure and its exponent for 3D irregular shape model. The model gives an exponent of 3.7e5 hence $\alpha L^2 = 30.23$ according to its geometry.**

**Table 13 Simulation results for 3D irregular shape.**

| Parameter | Value |
|---|---|
| $\alpha$ (1/m$^2$) | 0.43 |
| $\alpha L^2$ | 30.23 |
| Equilibrium pressure (psia) | 999.987 |
| % pressure deviation | 0.001% |

From the simulation results in table 13, the numerical-estimated shape factor, $\alpha L^2$ is 30.23, again, L denotes the cubic root of matrix volume as suggested in equation (11). The results also show that the final equilibrium deviates from initial pressure for only 0.001% so the constant pressure condition is maintained.

## Scaling laws for a generic shape factor: 3D and 2D geometry

As previously suggested, the usefulness of the scaling law is to obtain a universal constant for dimensionless shape factor which can apply to any shape without the need of fine-grid numerical simulation. Among the various scaling laws experiments from previous section (table 7), the two best dimensionless factor that give a minimum deviation is $\alpha \, \Delta l \, \frac{V}{S}$ and $\alpha L^2$ respectively. Therefore, these two scaling factors ($\alpha \, \Delta l \, \frac{V}{S}$ and $\alpha L^2$) are additionally applied to 3D geometry as well. Equation (11) and (12) define a characteristic length ($\Delta l$) for scaling; in 3D geometry, $\Delta l$ and $L$ are a cubic root of volume ($V$) and $S$ represents outer surface area of the matrix block. Table14 shows a comparison of two scaling laws i.e. $\alpha \, \Delta l \, \frac{V}{S}$ and $\alpha L^2$ for 2D and 3D geometry including that of the irregular shape blocks.

**Table 14 Scaling laws to estimate dimensionless shape factor of different geometries for 2D and 3D model including the irregular shape**

| Matrix Shape | $\alpha L^2$ | $\alpha \cdot \Delta l$ (V/S) | Deviation from average | |
|---|---|---|---|---|
| | | | $\alpha L^2$ | $\alpha \cdot \Delta l$ (V/S) |
| Square | 19.63 | 4.91 | -24% | -2% |
| Isosceles right triangle | 24.64 | 5.10 | -5% | 2% |
| Circle | 17.99 | 5.08 | -31% | 1% |
| Irregular shape2D | 26.42 | 4.54 | 2% | -9% |
| 3D cube | 29.15 | 4.86 | 12% | -3% |
| 3D square pyramid | 33.33 | 5.57 | 29% | 11% |
| 3D Irregular | 30.23 | 5.02 | 17% | 0% |
| average | 25.91 | 5.01 | | |
| standard deviation | 5.60 | 0.31 | | |
| S.D. and mean % diff. | *22%* | *6%* | | |

According to the table, if $\Delta l \frac{V}{S}$ is used as a scaling parameter, the dimensionless shape factor varies between 4.54 and 5.57 for the 2D irregular shape and 3D square pyramid that is a deviation of -9 and 11% respectively. This scaling factor gives the standard deviation of 6%. If $L^2$ is used instead, the standard deviation goes up to 22% while the variation of the factor varies between 17.99 and 33.33 for circle and 3D square pyramid that is the deviation of -31 and 29% respectively. Note that the average value of the dimensionless factor is almost the same as that of the 3D irregular shape i.e. 5.01 and 5.02 respectively.

Overall, it can conclude that using $\alpha \cdot \Delta l \frac{V}{S}$ as a scaling parameter gives the most confident value, the dimensionless shape factor derived from this method is $\alpha \cdot \Delta l \frac{V}{S} = 5.0$ with a maximum error of 10%.

## Discussion

The numerical-derived pressure responses have shown that, when matrix-fracture flow behaviour is governed by linear pressure diffusion equation under pseudo steady-state condition and constant boundary pressure, the shape factor ($\alpha$) depends on the matrix block's geometry. To be more precise, it depends largely on fracture spacing ($L$), matrix's surface area ($S$), its volume ($V$) and geometry's characteristic length ($\Delta l$) according to the scaling laws. Another observation is that different geometries have different $\alpha$ because of their different surface-to-volume ratio. A classic example is a comparison between square and circular shapes of the same area (from eq. 12: same $\Delta l$ as well); the circle always has shorter perimeter implying that the circle has lower sure face-to-volume ratio ($S/V$) and hence higher $V/S$. As a result, the circle always has higher $\alpha \cdot \Delta l \frac{V}{S}$ than the square, as shown in table 14. From this idea, therefore, the matrix of the same shape and size should give the same dimensionless shape factor because of the constant surface-to-volume ratio.

**Simulation models for different open-to-flow area of the same matrix block**

To test this assumption, three identical 20x20 square shape models were constructed with the same *L, A* and *V* -the only difference is experimented parameter i.e. area-opened-to-flow. In other words, three identical models have the same geometry but different area-opened-to-flow ratio ($f_{wet}$). In addition, the 20x20 2D square model of the previous section is used as a controlled experiment. The different models as shown in figure20 have the same parameters as tabulated in table1 in the previous section.
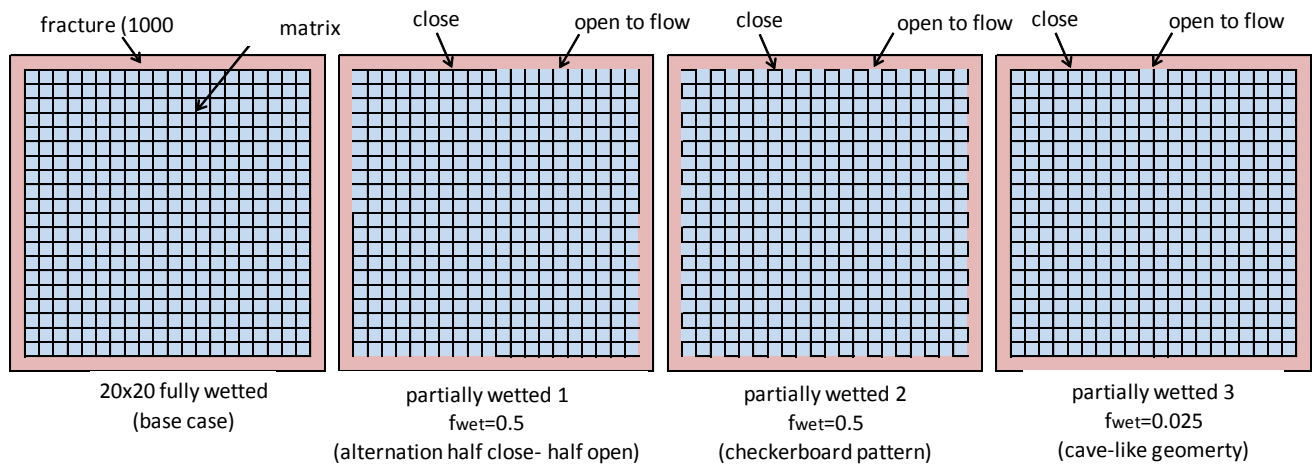


**Figure 20 Simulation models for differently-wetted matrix's outer surface. The base case has fully-wetted area while another two cases have the same $f_{wet}$ ratio but different formations ($f_{wet}$ =0.5) and the last model represents cave-like geometry where only little area is opened to flow ($f_{wet}$=0.025).**
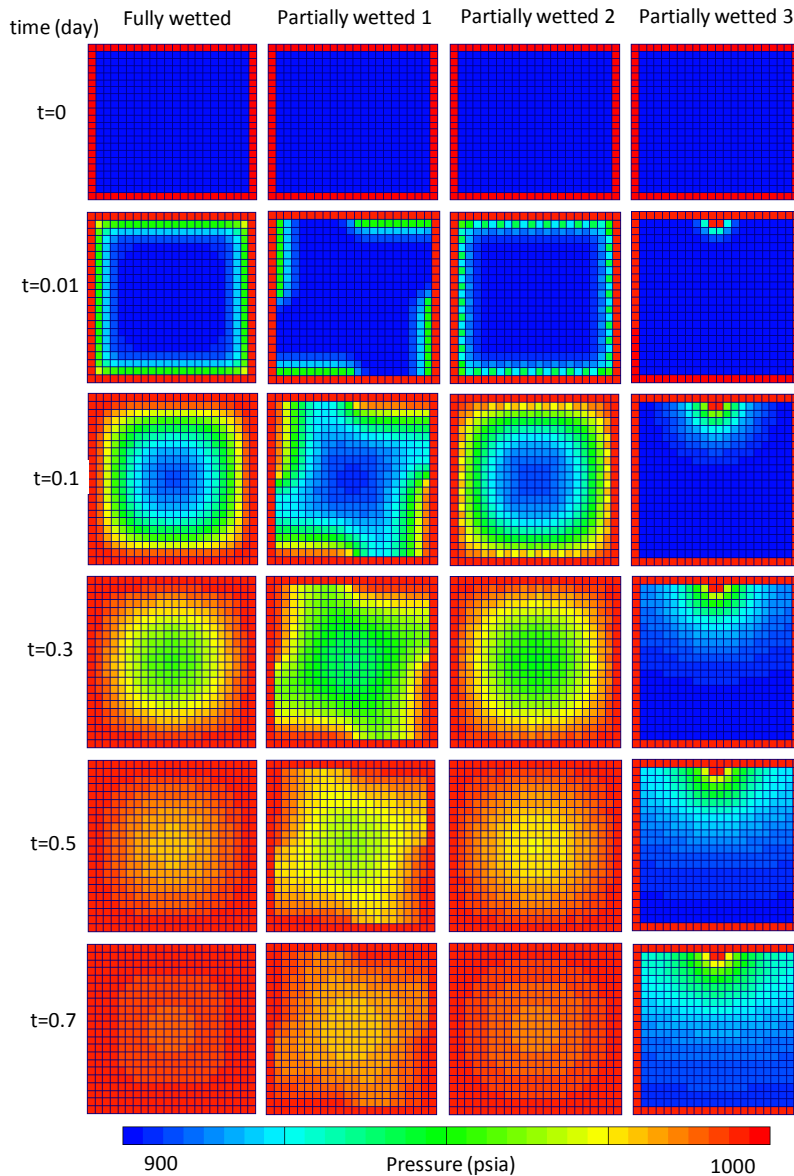
<div align="center">

| time (day) | Fully wetted | Partially wetted 1 | Partially wetted 2 | Partially wetted 3 |
|---|---|---|---|---|
| t=0 | | | | |
| t=0.01 | | | | |
| t=0.1 | | | | |
| t=0.3 | | | | |
| t=0.5 | | | | |
| t=0.7 | | | | |

</div>

900                              Pressure (psia)                              1000

**Figure 21 pressure diffusion for different partially wetted model. The model's physical properties are the same as presented in table 1.**

From the results, the base case model where the outer surface is fully opened gives the fastest pressure diffusion. The model quickly reaches pressure equilibration ($t \geq 0.7$ day) compared to partially-wetted models as illustrated in figure 21. From this figure, the models were put at the same initial condition. As the time progresses, pressure starts to diffuse through the opened cells as can be seen in the figure. Note that the diffusion patterns are different for wet1 and wet2 models despite the same area-opened-to-flow ($f_{wet}=0.5$). For wet1, the pressure diffuses through the opened cells and encircles the closed part resulting in a cyclone-like pattern. For wet2, the checker board shape, the diffusion pattern is very similar to the fully wetted model due to the fact that the flow path is less tortuous compared to that of wet1. Therefore, the diffusion is smoother and faster as can also be observed from figure 22. It is confirmed that wet2 reaches pressure equilibration at almost the same time as fully wetted and faster than wet1. From the figure at time $t=0.7$; the pressure for wet2 and fully wetted almost reaches the final pressure (red) whereas wet1 still have some yellow zone in middle part which means the pressure is still far from final equilibration. For wet3; it is clear that the pressure diffuses very slowly since the area-opened-to-flow is small ($f_{wet}=0.025$). The diffusion pattern is similar to a semi-circle front because of the symmetry. It takes more than 20 days to reach the equilibrium while other models reach the final state within 3 days.
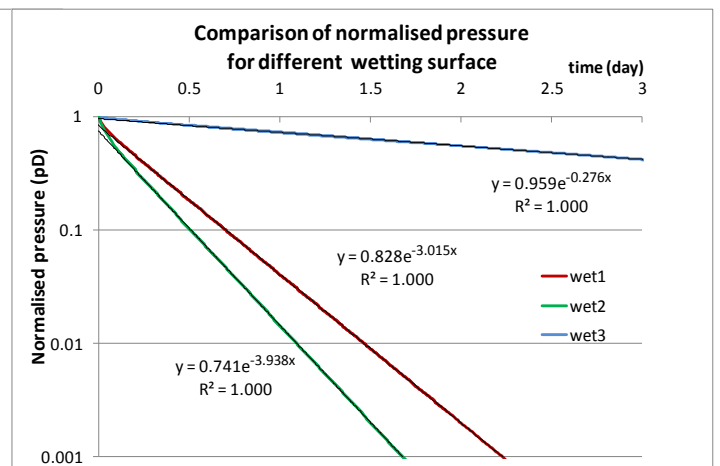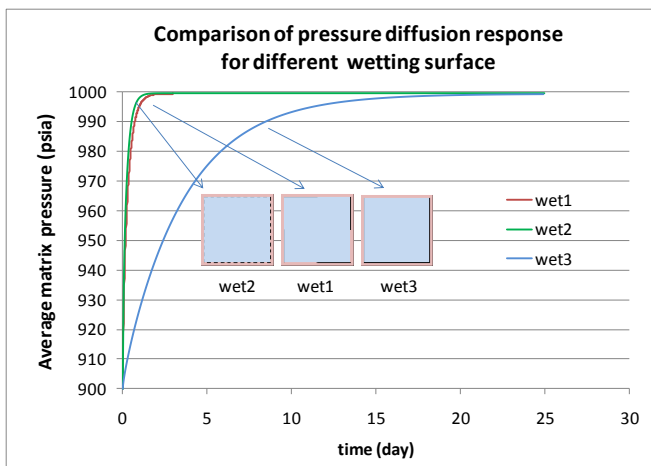


**Figure 22 comparison of pressure diffusion response for different model**   **Figure 23 comparison of normalised pressure for different wetting models**

As discussed that the pressure diffusion for wet1 is slower than wet2 despite the same the same area-opened-to-flow ($f_{wet}=0.5$), due to the fact that its flow path is more tortuous. Figure 22 also illustrated this response as can see that wet2 (green)

diffuses faster and reaches equilibrium (about t=3days) faster than wet1 where as it takes much longer for wet3 which is an extreme case. Therefore, the normalized pressure for wet3 gives the smallest slope, followed by wet1 and wet2 respectively, as shown in figure 23. As a result, wet3 has the smallest shape factor ($\alpha$), next came wet1, wet2 and fully wet models respectively. Table 15 shows these results as accordingly described, in addition, the scaling laws were tested on these partially opened surface models. All parameters were used in the same way as previously described except that the surface area of the matrix being modified by an area-opened-to-flow ratio ($f_{wet}$). This modified surface area ($\Pi_{wet}$) is expressed as follow;

$$\Pi_{wet} = f_{wet} \cdot \Pi \qquad\qquad (13)$$

According to table 15, the shape factor ($\alpha$) for wet2 is very close to fully wet model (12% deviation) as they have similar pressure diffusion. However, when the scaling laws of $\Pi_{wet}$ are applied, the deviation is larger. This is due to the surface opened to flow area of wet2 is suppressed while the pressure diffusion for the two cases are similar. In addition, the deviation of $\alpha$ between wet1 and fully wet is higher but becomes smaller when scaled by $\Pi_{wet}$; these are clearly shown in the last three column of the table. For the case of wet3, where $f_{wet}$ is very small, although the shape factor ($\alpha$) is smaller by one order of magnitude (E-6 vs. E-5), the usefulness of scaling factor $\alpha \cdot \Delta l \frac{V}{S}$ brings it to the same order (11.80 vs. 8.44 for wet3 and wet2 respectively).

For the case of partially wetted surface, although the scaling factor $\alpha \cdot \Delta l \frac{V}{S}$ does not give as confident value as that of fully opened, the factor is instructive in showing how the different wetting surface influences the shape factor and most importantly, it gives value of the same order of magnitude. These results show that the shape factor depends not only on geometrical factors i.e. surface-to-volume ratio ($S/V$), characteristic length ($\Delta l$) and area-opened-to-flow ratio ($f_{wet}$), it also depends on the physics of pressure diffusion within the matrix blocks.

**Table 15 Scaling laws to estimate dimensionless shape factor for different wetting matrix outer surface**

| Matrix Shape | $\alpha$ (m$^{-2}$) | Area (L$^2$) (m$^2$) | Perimeter ($\Pi$) (m) | $f_{wet}$ | Perimeter opened to flow ($\Pi_{wet}$), (m) | $\alpha L^2$ | $\alpha \Pi_{wet}^2$ | $\alpha (A/\Pi_{wet})^2$ | $\alpha (A^{1.5}/\Pi_{wet})$ or $\alpha \cdot \Delta l \frac{V}{S}$ |
|---|---|---|---|---|---|---|---|---|---|
| fully wet | 5.19E-5 | 3.72E+5 | 2.44E+3 | 1 | 2.44E+3 | 19.28 | 308.46 | 1.20 | 4.82 |
| wet1 | 3.48E-5 | 3.72E+5 | 2.44E+3 | 0.5 | 1.22E+3 | 12.93 | 51.71 | 3.23 | 6.46 |
| wet2 | 4.54E-5 | 3.72E+5 | 2.44E+3 | 0.5 | 1.22E+3 | 16.89 | 67.54 | 4.22 | 8.44 |
| wet3 | 3.18E-6 | 3.72E+5 | 2.44E+3 | 0.025 | 6.10E+1 | 1.18 | 0.01 | 118.02 | 11.80 |

## Conclusion

From this study, the numerical-estimated shape factors are verified with the known analytical values. The results are tabulated in this table. The shape factor for irregular shapes are numerically estimated and made dimensionless with the scaling factor $\alpha \cdot \Delta l \frac{V}{S}$. This shape factor gives the most confident value of $\boldsymbol{\alpha \cdot \Delta l \frac{V}{S} = 5.0}$ with an error less than 10%. The variable $\frac{V}{S}$ denotes volume-to-surface ratio of the matrix blocks and $\Delta l$ represents a characteristic length that similar to the mean radius of the pressure field; it is defined as $\Delta l \equiv \sqrt[2]{A}$ for 2D shape and $\Delta l \equiv \sqrt[3]{V}$ for 3D shape. While, the conventional dimensionless shape factor using fracture spacing or area of the matrix block ($\alpha L^2$) gives more than 30% deviation. This scaling law suggests that shape factor depends largely on surface-volume ratio ($S/V$) and the characteristic length $\Delta l$.

**Table 16 Numerical-estimated shape factor for standard shapes compare to analytical solution**

| Matrix shape | Description | $\alpha \cdot \Delta l \frac{V}{S}$ Analytical solution | $\alpha \cdot \Delta l \frac{V}{S}$ Numerical-estimated | Difference % |
|---|---|---|---|---|
| | Square (Two normal fractures) | 4.94 | 4.91 | 0.56 |
| | Circle (Radial geometry parallel pipe) | 5.13 | 5.08 | 0.97 |
| | Isosceles right triangle | 5.11 | 5.10 | 0.12 |
| | 3D cube (Three fracture sets) | 4.94 | 4.86 | 1.5 |
| **Any shape** | | $\alpha \cdot \Delta l \frac{V}{S} = 5.0$ | | |

An analysis on pressure diffusion for different wetting surface area suggested that the shape factor does not only depend on geometrical factors i.e. surface-to-volume ratio ($S/V$), characteristic length ($\Delta l$) and area-opened-to-flow ratio ($f_{wet}$), but it also depends on the physics of pressure diffusion within the matrix blocks.

## Suggested future work

This work is done based on a linear diffusion equation with the pseudo steady-state assumption. To understand the physics of flow behaviour more precisely, it is suggested to extend the work to include the non-linear term in a transient flow regime. In addition, a multi-phase matrix-fracture flow and the non-Darcy flow should provide more insights of pressure diffusion behaviour for the system. Finally, an investigation on a characteristic length representing centriod of pressure field for each flow regime (for every time step) may give a universal scaling law more accurately.

## Nomenclature

| | |
|---|---|
| $\alpha$ | shape factor $(1/m^2)$ |
| $\alpha L^2$ | dimensionless Shape factor based on fracture spacing (or area) |
| $\alpha \cdot \Delta l \frac{V}{S}$ | dimensionless Shape factor based on scaling parameter $\Delta l \frac{V}{S}$ |
| $A$ | area $(m^2)$ |
| $c_f$ | fluid compressibility $(1/psia)$ |
| $c_m \ and \ c_p$ | rock compressibility $(1/psia)$ |
| $c_t$ | total compressibility $(1/psia)$ |
| $k_m$ | matrix permeability $(mD)$ |
| $k_f$ | fracture permeability $(mD)$ |
| $\Delta l$ | characteristic length; for 2D: $\Delta l \equiv \sqrt[2]{A}$ ; for 3D: $\Delta l \equiv \sqrt[3]{V}$ |
| $Lx, Ly, Lz$ | fracture spacing in x, y and z direction |
| $\Pi$ | perimeter $(m)$ |
| $\emptyset_f$ | fracture porosity |
| $\emptyset_m$ | matrix porosity |
| $pD$ | normalised pressure (dimensionless) |
| $p_f$ | fracture pressure $(psia)$ |
| $\bar{p}_m$ | average matrix pressure $(psia)$ |
| $q_{mf}$ | matrix-fracture flow rate he fractures per unit volume $(1/s)$ |
| $Q$ | flow rate $(m^3/s)$ |
| $S$ | outer-surface area $(m^2)$ |
| $\mu$ | viscosity $(c.p.)$ |
| $V$ | volume $(m^3)$ |

## References

Barenblatt, G.I., Zheltov, Iu.P. and Kochina, I.N. (1960) Basic concepts in the theory of seepage of homogeneous liquids in fissured rocks (Strata). *Journal of Applied Mathematics and Mechanic, Vol. 24, No.5, pp 852-864, 1960.*

Coats, K.H. (1989) Implicit compositional simulation of single-porosity and dual-porosity reservoirs. *Society of Petroleum Engineers, SPE 18427, 1989.*

Diete, A. and Zimmerman, R.W. (2009) Shape factors for irregularly-shaped matrix blocks. *A report submitted in partial fulfilment of the requirement for MSc in Petroleum Engineering, Department of Earth Science and Engineering, Imperial College London, 2009.*

Gottlieb H.P.W. (1988) Eigenvalues of the Laplacian for rectilinear regions. *Journal of Australian Mathematical Society, ser. B29, pages 270-281, 1988.*

Kazemi, H., Merrill Jr, L.S., Porterfield, K.L. and Zeman, P.R. (1976) Numerical simulation of water-oil flow in naturally fractured reservoir. *Society of Petroleum Engineers journal, SPE 5719, 1976.*

Lim, K.T. and Aziz, K. (1995) Matrix-fracture transfer shape factors for dual-porosity simulators. *Journal of Petroleum Science and Engineering, Vol. 13, Pages 169-178, 1995.*

Mathias, S.A. and Zimmerman, R.W. (2003) Laplace transform inversion for late-time behavior of groundwater flow problems. *Water Resources Research, Vol. 39, No. 10, Pages 1283, 2003.*

Mora, C.A., Wattenbarger, R.A.(2009) Analysis and verification of dual porosity and CBM shape factors. *Journal of Canadian Petroleum Technology, Vol. 48, No. 2, 2009.*

Warren, J.E. and Root, P.J. (1963) The behavior of naturally fractured reservoirs. *Society of Petroleum Engineers journal, SPE 426, 1963.*

Yeo, In-Wook., Zimmerman, R.W. (2000) Accuracy of the renormalization method for computing effective conductivities of heterogeneous media. *Transport in Porous Media 45: 129–138, 2001.*

Zimmerman, R.W., Chen, G., Hadgu, T. and Bodvarsson, G.S. (1993) A numerical dual-porosity model with semi-analytical treatment of fracture/matrix flow. *Water Resources Research, Vol. 29, No. 7, Pages 2127-2137, 1993.*

Zimmerman, R.W. and Bodvarsson, G.S. (1995) Effective block size for imbibition or absorption in dual-porosity media. *Geophysical Research Letters, Vol. 22, No. 11, Pages 1461-1464, 1995.*